Article

Inter-Eye Association of Visual Field Defects in Glaucoma and Its Clinical Utility

Bettina Teng[1,*], Dian Li[1,2,*], Eun Young Choi[1,*], Lucy Q. Shen[3], Louis R. Pasquale[4,5], Michael V. Boland[6], Pradeep Ramulu[7], Sarah R. Wellik[8], Carlos Gustavo De Moraes[9], Jonathan S. Myers[10], Siamak Yousefi[11], Thao Nguyen[12], Yuying Fan[1], Hui Wang[1,13], Peter J. Bex[14], Tobias Elze[1,15], and Mengyu Wang[1]

[1] Schepens Eye Research Institute of Massachusetts Eye and Ear, Harvard Medical School, Boston, MA, USA
[2] Department of Data Sciences, Dana-Farber Cancer Institute and Harvard T.H. Chan School of Public Health, Boston, MA, USA
[3] Massachusetts Eye and Ear, Harvard Medical School, Boston, MA, USA
[4] Eye and Vision Research Institute of New York Eye and Ear at Mount Sinai, Icahn School of Medicine at Mount Sinai, New York, NY, USA
[5] Channing Division of Network Medicine, Brigham and Women's Hospital, Harvard Medical School, Boston, MA, USA
[6] Wilmer Eye Institute and Division of Health Sciences Informatics, Johns Hopkins University School of Medicine, Baltimore, MD, USA
[7] Wilmer Eye Institute, Johns Hopkins University School of Medicine, Baltimore, MD, USA
[8] Bascom Palmer Eye Institute, University of Miami School of Medicine, Miami, FL, USA
[9] Edward S. Harkness Eye Institute, Columbia University Medical Center, New York, NY, USA
[10] Wills Eye Hospital, Thomas Jefferson University, Philadelphia, PA, USA
[11] Hamilton Eye Institute, University of Tennessee Health Science Center, Memphis, TN, USA
[12] Department of Mechanical Engineering, Johns Hopkins University, Baltimore, MD, USA
[13] Institute for Psychology and Behavior, Jilin University of Finance and Economics, Changchun, China
[14] Department of Psychology, Northeastern University, Boston, MA, USA
[15] Max Planck Institute for Mathematics in the Sciences, Leipzig, Germany

Purpose: To investigate intereye associations of visual field (VF) defects.

Methods: We selected 24-2 VF pairs of both eyes from 63,604 patients tested on the same date with mean deviation (MD) ≥ -12 dB. VFs were decomposed into one normal and 15 defect patterns previously identified using archetypal analysis. VF pattern weighting coefficients were correlated between the worse and better eyes, as defined by MD. VF defect patterns (weighting coefficients $> 10\%$) in the better eye were predicted from weighting coefficients of the worse eye by logistic regression models, which were evaluated by area under the receiver operating characteristic curve (AUC).

Results: Intereye correlations of archetypal VF patterns were strongest for the same defect pattern between fellow eyes. The AUCs for predicting the presence of 15 defect patterns in the better eye based on the worse eye ranged from 0.69 (superior nasal step) to 0.92 (near total loss). The AUC for predicting superior paracentral loss was 0.89. Superior paracentral loss in the better eye was positively correlated with coefficients of superior paracentral loss, central scotoma, superior altitudinal defect, nasal hemianopia, and inferior paracentral loss in the worse eye, and negatively correlated with coefficients of the normal VF, superior peripheral defect, concentric peripheral defect, and temporal wedge. The parameters are presented in the descending order of statistical significance.

Conclusions: VF patterns of the worse eye are predictive of VF defects in the better eye.

Translational Relevance: Our models can potentially assist clinicians to better interpret VF loss under measurement uncertainty.

1

Introduction

Glaucoma diagnosis and monitoring are based on both structural and functional assessments, which can be affected by individual eye anatomy variations.[1–7] Prior work has leveraged the asymmetry or symmetry in glaucomatous damage between eyes to make a disease diagnosis.[8] Intereye differences in optic disc characteristics,[9–11] retinal nerve fiber layer thickness,[12–15] intraocular pressure,[16–21] and visual field (VF) sensitivity[19,22–24] have been suggested as markers of early glaucoma. Although it is known that VF sensitivities between fellow eyes are correlated, it remains largely inconclusive whether VF loss is more likely to occur in the same or different regions.

Understanding correlation in VF loss patterns between fellow eyes of glaucoma patients is a subject of both clinical and scientific significance. Clinically, if there are high correlations in patterns of VF loss between fellow eyes, it would be feasible to use VF features of one eye to predict the VF loss defect present in the fellow eye. The predictive model could help clinicians better determine whether a defect in the better eye is real or the result of random fluctuation and decide whether a confirmatory or supplemental test should be done sooner. For example, a central VF defect can often be missed on the 24-2 pattern and requires a 10-2 VF test to detect the damage.[25] Furthermore, understanding intereye correlations can inform patients about the likely course of disease, for instance, if glaucomatous paracentral loss in one eye will be followed by a similar pattern of loss in the fellow eye. From a research perspective, the question of whether VF loss patterns are related between eyes is important because of its implications for pathophysiology. There is ongoing debate regarding the etiology (e.g., biomechanical, vascular, and genetic risk factors) of optic nerve damage in glaucoma.[26–30] High intereye correlation in patterns of functional loss would suggest that individual patients harbor unique systemic susceptibilities[31–35] (e.g., genetic and environmental) to developing the same type of damage in both eyes as opposed to local eye-specific factors (e.g., intereye variations of myopia severity and optic nerve head architecture) leading to unilateral or different types of VF damage to each eye.

In a prior study, it has been reported that there are fairly high correspondence rates of VF loss within the same superior or inferior hemifield between fellow eyes.[36] The prior study suggests that VF loss might be more likely to occur in the same locations in fellow eyes, although the measure used was hemifield-wise quantification, which was less optimal to precisely quantify regional VF loss.

In this study, we have used an unsupervised artificial intelligence tool termed archetypal analysis to precisely quantify regional VF defects and investigate the inter-eye correlations of regional VF defects. We have further developed models to predict the presence of defects in the better eye from the VF pattern of the worse eye in patients with mild to moderate glaucoma. We have shown our model details focusing on paracentral defects given their major functional consequence.[37,38]

Methods

The VF data used in this study were collected and managed by the Glaucoma Research Network, a consortium composed of Massachusetts Eye and Ear, Wilmer Eye Institute, New York Eye and Ear Infirmary of Mount Sinai, Bascom Palmer Eye Institute, Wills Eye Hospital, and Hamilton Eye Institute. The institutional review boards (IRB) of each ophthalmic center approved the creation of the database in this retrospective study. The IRB for this specific study was approved by Massachusetts Eye and Ear. Because of the retrospective nature of this study, the IRB waived the need for informed consent of patients. This study complies with all principles of the Declaration of Helsinki.

Participant and Data

We included reliable VFs from our large dataset of Swedish Interactive Thresholding Algorithm Standard 24-2 VFs measured with the Humphrey Field Analyzer (Carl Zeiss Meditec, Dublin, CA, USA). The VF data were directly exported from the Humphrey Field Analyzer device using the Zeiss advanced license for research. The reliability criteria were fixation loss $\leq$ 33%, false-negative rates $\leq$ 20%, and false-positive rates $\leq$ 20%.[39] The cutoffs for fixation loss and false-positive rates are based on published recommendations,[40,41] and the cutoff for false-negative rates is based on the criterion used to develop archetype analysis[42] and has been adapted for glaucoma identification in population-based studies.[43,44]

We selected the most recent VF pairs of both eyes from each subject. The worse eye was defined as the eye with the lower mean deviation (MD). To focus on mild and moderate stage glaucoma, only pairs of eyes with MD equal to or better than -12 dB in both eyes were included in our data analyses. VFs with MD equal or greater than $+2$ dB were excluded from
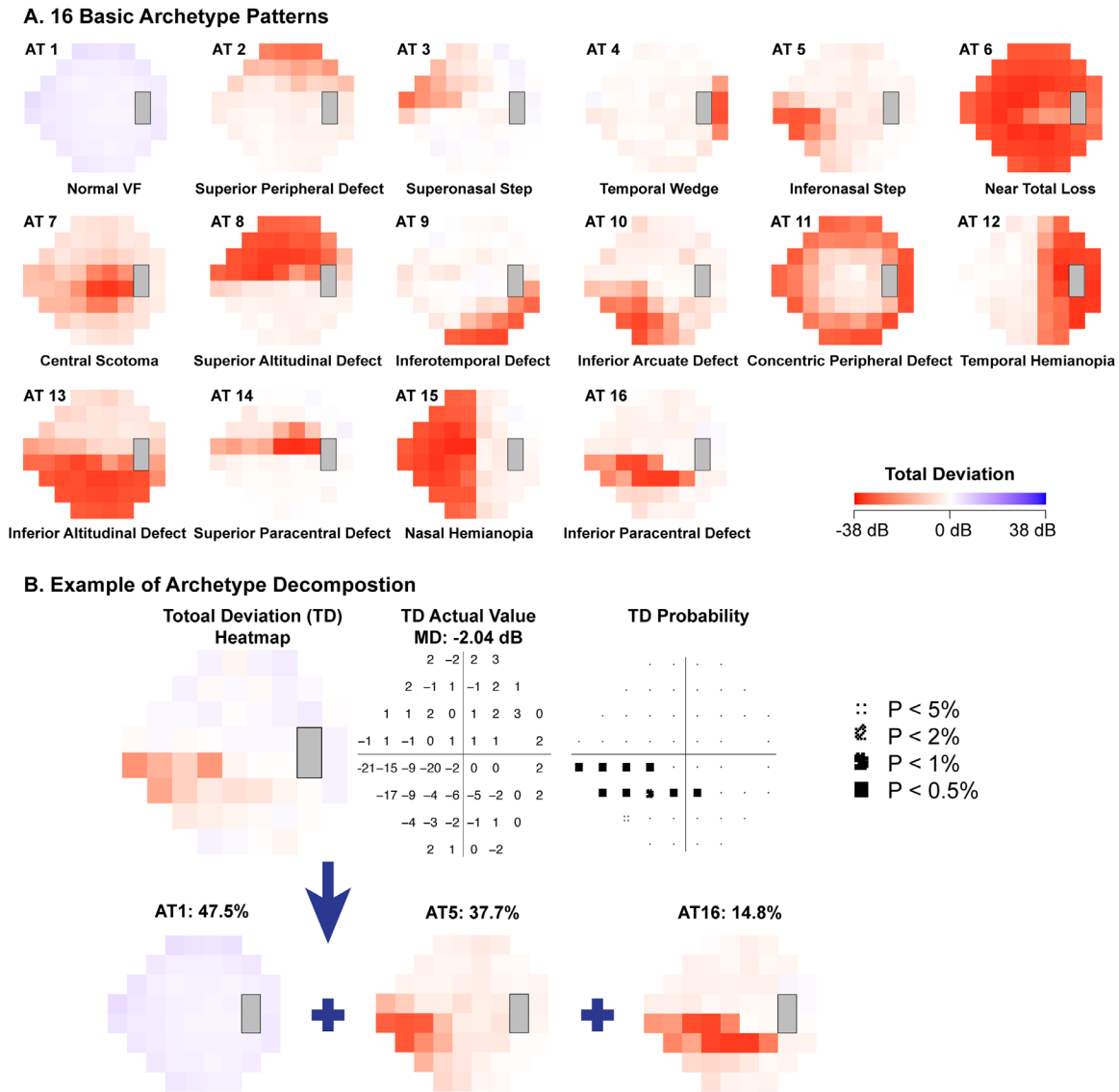
Figure 1. (**A**) An illustration of the 16 archetype (AT) patterns and corresponding nomenclature derived by artificial intelligence and clinically validated in our prior work.[42,46] (**B**) An example of the AT decomposition method using the total deviation (TD) plot. The plotting range is set from −38 dB to +38 dB to ensure that on the color scale white represents normal visual field sensitivities with 0 dB.

analysis because of the likelihood of high false-positive test responses not captured despite applying the cutoff for false-positive rates mentioned above.

Statistical Analyses

Each total deviation (TD) plot was decomposed into 16 archetypal patterns including one normal VF pattern and 15 defect patterns determined in our prior work,[42] which were clinically validated in a subsequent study[45] and further applied to improve glaucoma diagnosis and progression detection.[39,46–48] An illustration of the 16 archetype (AT) patterns and corre-

sponding nomenclature can be found in Figure 1A. An example of VF decomposition into ATs is shown in Figure 1B. The TD plots of the left eyes were mirrored to match the orientation of the right eye. We used R language to plot all the results of VF analyses in this work.[49]

Pearson correlations were calculated between the TD values of the better and worse eyes at each of the 52 locations of the 24-2 VF in the temporal nasal coordinate system. In addition, intereye Pearson correlations of the VF defect pattern weighting coefficients for ATs 2 to 16 were calculated. *P* values were adjusted for multiple comparisons using the false discovery rate method.[50]
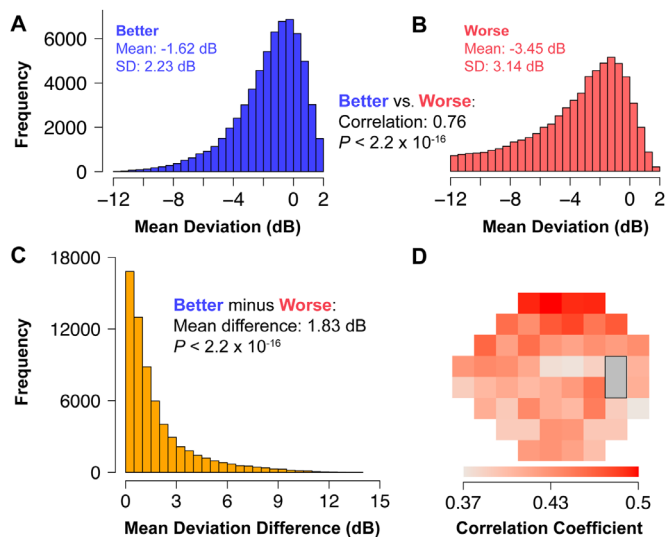
Figure 2. Distribution of mean deviation (MD) values for the better (**A**) and worse (**B**) eyes. Pearson correlation coefficient of MD values between the better and worse eyes is shown in the legend. (**C**) Distribution of MD difference (better minus worse eyes). (**D**) Pearson correlation coefficients of total deviation (TD) values between the better and worse eyes at each of the 52 test locations on the 24-2 visual field. *Darker red* means stronger correlation.

Subsequently, logistic regression was applied to calculate the probability that a particular VF defect pattern exists in the better eye using the VF pattern coefficients of the worse eye. The presence of a VF defect was defined as a defect AT (ATs 2 to 16) weighted greater than 10% of the total. Stepwise regression using Bayesian information criterion (BIC) was performed to select the optimal combination of VF patterns in the worse eye to calculate the probability of the presence of a VF defect in the better eye. Tenfold cross-validation was applied to evaluate the performance of the models with area under the receiver operating characteristic curve (AUC) with 95% confidence intervals. In total, 15 AUC values were calculated for predicting each of 15 VF defect patterns in the better eye.

Results

In all, 63,604 pairs of VFs with MD ≥ -12 dB but $< +2$ dB from 63,604 patients (mean age 61.0 $\pm$ 16.7 years) were selected for data analyses. MD ranged from -11.8 to 2.0 dB and -12.0 to 2.0 dB for better and worse eyes, respectively (Figs. 2A and 2B). The average MD of the better eyes (-1.6 ± 2.2 dB) was significantly better ($P < 0.001$) than that of the worse eyes (-3.5 ± 3.1 dB, Fig. 2C). The Pearson correlation coefficient between MD values of the better and the worse eyes was 0.76 ($P < 0.001$).
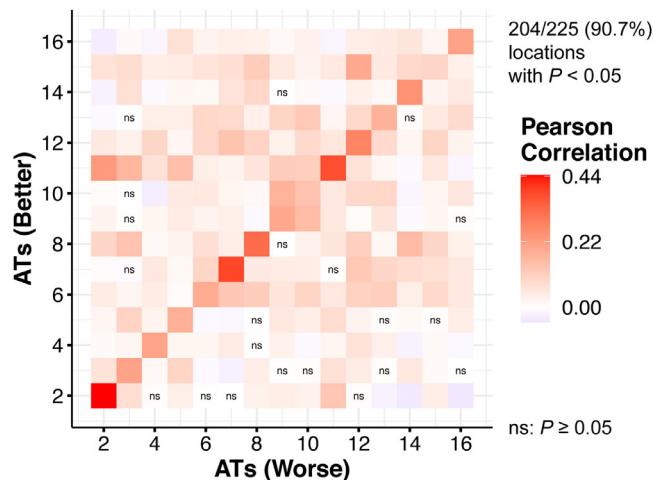

Figure 3. Pearson correlation coefficients between the 15 decomposed archetypes (ATs) representing defect patterns in the better (*vertical axis*) and worse (*horizontal axis*) eyes. Darker red means stronger correlation. Correlation was marked as nonsignificant (ns) on the heatmap if the corresponding *P* value ≥ 0.05. *P* values were corrected for multiple comparisons.

The maximum intereye correlations (Pearson correlation coefficient r) between the TDs at each of the 52 locations were located in the superior rim, whereas the minimum coefficient was located in the superior paracentral region (*r* range: 0.37 to 0.50, $P < 0.001$, Fig. 2D). In general, stronger correlations occurred in the upper hemifield. The weaker *r*-coefficients were located in the inferotemporal and inferior arcuate regions.

Figure 3 illustrates the Pearson correlation coefficients (p values were corrected for multiple comparisons) between the weighting coefficients of the 15 defect ATs in better (vertical axis) and worse eyes (horizontal axis). The highest correlations were seen between the same archetypal defect pattern in better-worse eye pairs (*r* range: 0.18–0.44), with the exception of two ATs: 9 (inferotemporal defect) and 15 (nasal hemianopia). AT 9 in the worse eye had the highest correlation with AT 10 (inferior arcuate defect) in the better eye (*r* = 0.17), and AT 12 in the worse eye had the highest correlation with AT 15 (nasal hemianopia) in the better eye (*r* = 0.19). The six ATs exhibiting highest correlations with the same decomposition pattern in the fellow eye were: AT 2 (superior peripheral defect, *r* = 0.44), AT 7 (central scotoma, *r* = 0.39), AT 11 (concentric peripheral defect, *r* = 0.37), AT 8 (superior altitudinal defect, *r* = 0.32), AT 12 (temporal hemianopia, *r* = 0.27), and AT 14 (superior paracentral defect, *r* = 0.25). More details for the correlation coefficients and *P* values can be found in Supplementary Table S1.
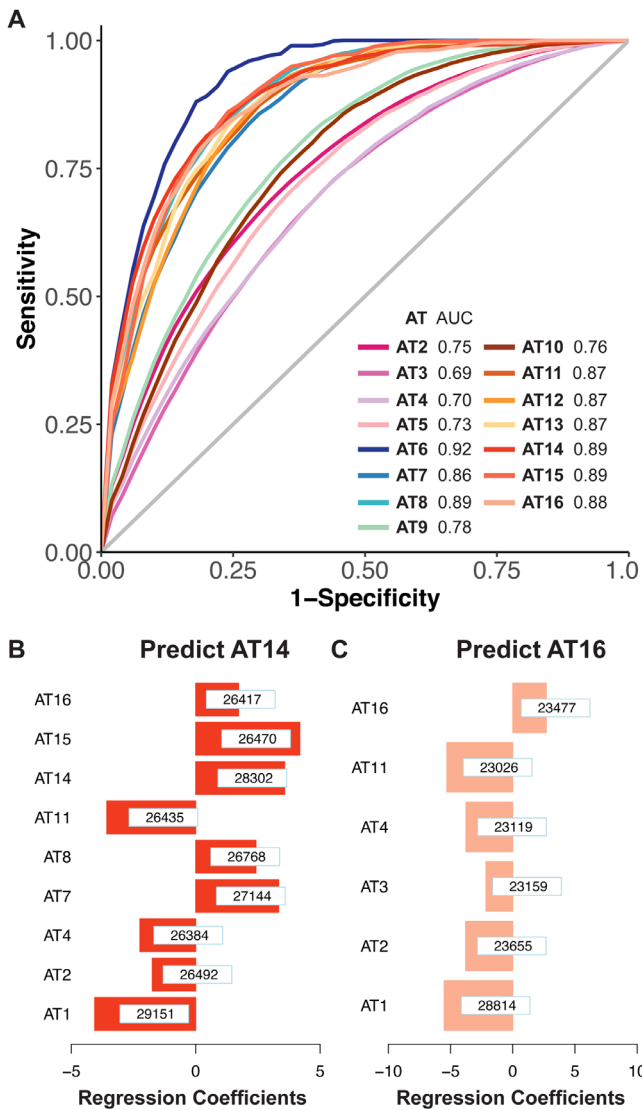
Figure 4. The best models selected by stepwise logistic regression to calculate the probability of the presence of archetypes (AT) 2 through 16. (**A**) AUCs with their mean values. (**B**, **C**) Logistic regression coefficients to predict the presence (>10%) of AT 14 (**B**) and AT 16 (**C**) in the better eye using the AT coefficients of the worse eye. The numbers noted on top of the bars represent the respective statistical significance of each parameter, which were measured by the magnitude of BIC increase when a parameter was removed from the optimal model. When the BIC increase for a parameter is at least 6 higher than another parameter in the model, the former parameter is considered strongly more associated with the outcome than the latter parameter.[51]

From the archetypal weighting coefficients in the worse eye, the best models were selected to calculate the probability of the presence of ATs 2 through 16 (weighting coefficients > 10%) in the better eye. Model performance was evaluated by AUC through 10-fold cross-validation (Fig. 4A). The AUC was greater than 0.80 for nine ATs: AT 6 (near total loss, AUC: 0.92), AT 14 (superior paracentral defect,

0.89), AT 8 (superior altitudinal defect, 0.89), AT 16 (inferior paracentral defect, 0.88), AT 11 (concentric peripheral defect, 0.88), AT 15 (nasal hemianopia, 0.88), AT 13 (inferior altitudinal defect, 0.87), AT 12 (temporal hemianopia, 0.87), and AT 7 (central scotoma, 0.86).

Next, we focused on modeling ATs representing paracentral loss, which most adversely affect the quality of life in glaucoma patients.[37,38] Figures 4B and 4C show the best models to predict the presence of AT 14 (superior paracentral defect) and 16 (inferior paracentral defect) in the better eye from the weighting coefficients in the worse eye. Superior paracentral defect (AT 14), central scotoma (AT 7), superior altitudinal defect (AT 8), nasal hemianopia (AT 15), and inferior paracentral defect (AT 16) in the worse eye were positively correlated with the presence of AT 14 in the better eye ($P < 0.05$). On the other hand, the normal VF (AT 1), superior peripheral defect (AT 2), concentric peripheral defect (AT 11), and temporal wedge (AT 4) in the worse eye were negatively correlated with the presence of AT 14 in the better eye ($P < 0.05$). In predicting inferior paracentral defects (AT 16), the same defect pattern (AT 16) in the worse eye was positively correlated ($P < 0.05$), while the normal VF (AT 1), superior peripheral defect (AT 2), superonasal step (AT 3), temporal wedge (AT 4), and concentric peripheral defect (AT 11) in the worse eye were negatively correlated with the presence of AT 16 in the better eye ($P < 0.05$). The parameters in the optimal models are presented in the descending order of the respective statistical significance measured by the magnitude of BIC increase when a parameter was removed from the optimal model. When the BIC increase for a parameter is at least six higher than another parameter in the model, the former parameter is considered strongly more associated with the outcome than the latter parameter.[51] For instance, in predicting superior paracentral loss (AT 14) in the better eye, the BIC increase for AT 14 (superior paracentral loss) was 1157 higher than the BIC increase for AT 7 (central scotoma). The specific models for predicting each of the 16 ATs can be found in Supplementary Figure S1.

Finally, we illustrate examples in which our model can be useful in clinical practice. We focused on the superior paracentral defect (AT 14) and inferior paracentral defect (AT 16), because paracentral loss is most detrimental to the quality of life of glaucoma patients.[37,38] In Figure 5, three consecutive VFs (each performed six months apart) are shown for the better and worse eyes of two patients. Figure 5A shows a patient who had archetype 14 as the dominant archetype in the worse eye. In the better eye, archetype
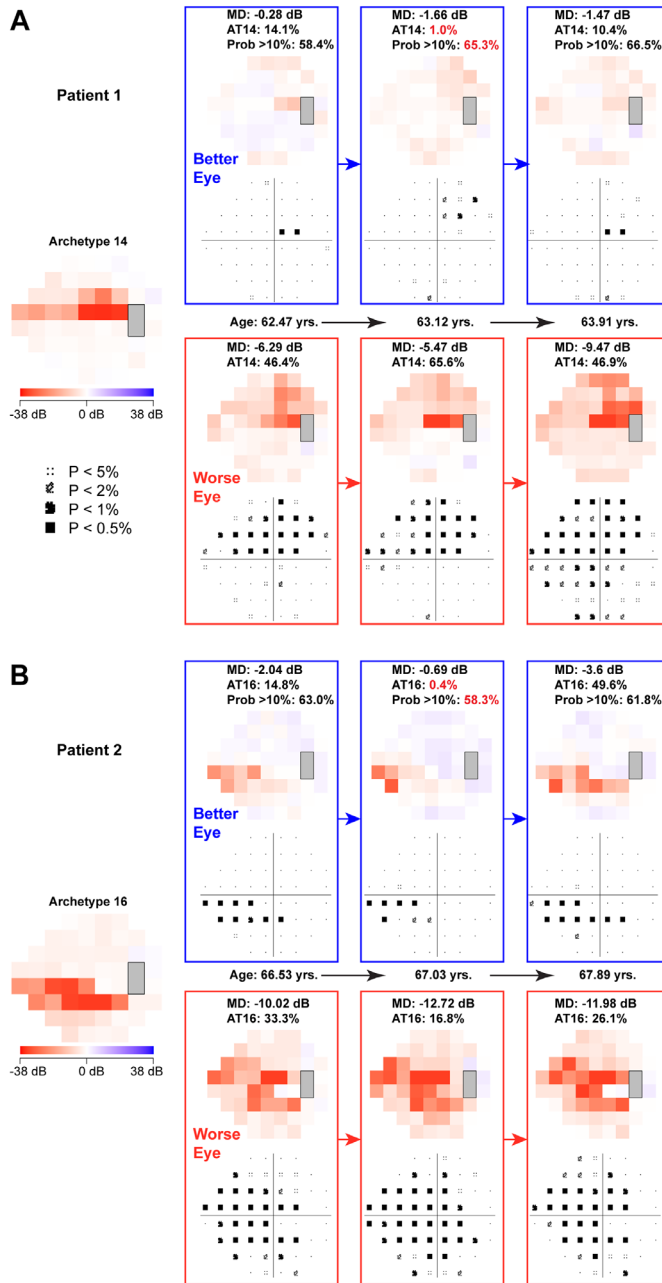
Figure 5. Three consecutive visual fields (VFs) of two patients, measured 6 months apart, in which the defect in the better eye (*blue box*) disappears in the second test (*middle column*) and reappears in the third test (*right column*). (**A**) Patient 1 has archetype 14 as the dominant VF defect; (**B**) Patient 2 has archetype 16 as the dominant VF defect. Our model estimates the presence of archetypes 14 and 16 (>10%) in the better eye with high probabilities at all three time points.

14 initially weighed 14.1% of the total VF, decreased to 1% on a subsequent test, and increased again to 10.4% six months later. Similarly, in Figure 5B, archetype 16 was the dominant archetype in the worse eye. In the better eye, archetype 16 initially weighed 14.8%, but decreased to 0.4% and then increased to 49.6% on

subsequent tests. Our model indicates that at each of the time points (at least 58.3% likelihood), archetypes 14 and 16 should have high probabilities to weigh more than 10% in the better eye of Patients 1 and 2, respectively. Using our model, clinicians can have increased confidence that a defect is likely to be present in the better eye even though it was not seen on the actual test. Supplementary Figure S2 shows additional examples in which our model may be informative of paracentral VF defects to be developed in the follow-up tests.

Discussion

In this work, we studied the intereye correlation of VF defects based on computationally derived archetypal VF patterns using a large multicenter dataset. We found that VF defects are more likely to occur in the same regions than different regions in fellow eyes (Fig. 3). Furthermore, we demonstrated that VF defect patterns in the better eye can be accurately predicted by VF loss patterns of the worse eye. Our results suggest that in situations of test-retest uncertainty, VF patterns of the worse eye may be used as a reference to aid clinicians better detect and interpret the paracentral VF loss in the better eye and decide whether a 10-2 test is needed. The strong symmetry of VF loss patterns observed also lends insight into the pathophysiology of glaucoma.

We found that among the 15 defect ATs, 13 of them were most strongly correlated with the same AT in the other eye. This suggests that pairs of eyes are more likely to have the same defect pattern than to have different patterns in each eye. These results are in line with those of Hoffman et al.[36] as discussed above, but our analysis significantly improves upon their work, as we utilized 15 computationally-derived AT patterns to quantify regional VF loss, compared with superior and inferior hemifield quantifications. Our results are also consistent with the prior findings that there were high concordance rates for structural defects in inferior and superior locations, which corresponds with typical patterns of early glaucomatous damage.[13] Exceptions to this paradigm were seen in the following: an inferior arcuate defect (AT 10) was correlated more with an inferotemporal defect (AT 9) than with itself ($r = 0.14$) in both worse-better ($r = 0.15$) and better-worse ($r = 0.17$) eye comparisons. Similarly, nasal hemianopia (AT 15) had a stronger or equal correlation with temporal hemianopia (AT 12) than with itself ($r = 0.10$) in both worse-better ($r = 0.10$) and better-worse ($r = 0.19$) eye comparisons. Interestingly, both of these combinations (ATs 12/15 and ATs 9/10) are

mirror images of each other, with symmetry across the vertical axis of the VF. The correlation between ATs 12 and 15 suggest the presence of homonymous hemianopia, whereas ATs 9 and 10 likely reflect the same regional pattern of glaucomatous optic nerve damage. Overall, our finding that VF defects present in one eye are most strongly correlated with the same type of defect pattern in the fellow eye implicates that systemic/inherited factors may play a central role on vision loss in glaucoma.

Given the overall intereye symmetry of VF patterns observed, we developed models to calculate the probability of the presence of VF defects in one eye based on the fellow eye. In this work, we used the worse eye as a reference for the better eye, because defects can disappear and reappear more often in the better eye than in the worse eye.[39] We empirically set 10% as the threshold ratio to label a VF pattern as a major defect. We found that a number of ATs, representing both glaucomatous and non-glaucomatous VF loss, can be estimated with a relatively high AUC (range, 0.86 to 0.92; Fig. 4A). These include superior altitudinal defect (AT 8, 0.89), inferior altitudinal defect (AT 13, 0.87), superior paracentral defect (AT 14, 0.89), and inferior paracentral defect (AT 16, 0.88), which are all associated with glaucomatous field loss; central scotoma (AT 7, 0.86), which is more typically seen in macular disorders; temporal (AT 12, 0.87) and nasal hemianopia (AT 15, 0.89), which occur in chiasmal and post chiasmal pathology; concentric peripheral defect (AT 11, 0.87), typically associated with rim artifacts due to hyperopic corrective lenses; and near total loss (AT 6, 0.92). The rest of the 15 VF defect patterns had lower AUC (range, 0.69 to 0.76; Fig. 4A) and included the superior peripheral defect (AT 2, 0.75), superonasal step (AT 3, 0.69), temporal wedge (AT 4, 0.70), inferonasal step (AT 5, 0.73), inferotemporal defect (AT 9, 0.78), and inferior arcuate defect (AT 10, 0.76).

The common characteristics of the latter VF archetypes are that they all represent early or mild VF loss in the peripheral region, while the former VF archetypes all had advanced VF loss or paracentral VF loss. The implications of the characteristic difference between the more predictable and less predictable archetypes relate to test-retest variability and disease pathophysiology. From the perspective of test-retest variability, prior studies reported that the test-retest variability is higher in the peripheral region compared with the paracentral region. Therefore it is reasonable that VF archetypes with peripheral loss subject to higher test-retest variability in the better eye were less predictable from the worse eye and VF archetypes with paracentral loss subject to lower test-retest variability were more predictable.[52,53] It is also known that test-

retest variability was higher in eyes with more severe VF loss in glaucoma. This appeared to be contradicted with our findings that the VF archetypes with more advanced VF loss were more predictable.[52,54,55] This may be explained by prior findings that the relationship between VF loss severity and test-retest variability was nonlinear.[56] Test-retest variability in VFs with early and advanced VF loss were relatively low and relatively high in VFs with moderate VF loss. From the perspective of disease pathophysiology, prior studies have shown that paracentral VF loss was related to systemic or genetic factors,[31–33] which in theory tend to affect both eyes. It is possible that some VF loss patterns are more related to systemic/inherited factors,[57,58] while some VF loss patterns are related to local eye-specific factors (e.g., intereye variations of myopia severity and optic nerve head architecture). The possible implications for glaucoma pathophysiology are discussed later in this work in detail. Furthermore, our findings that VF archetypes with more advanced VF loss were more predictable than those with early or mild VF loss might implicate that early VF loss is more random and asymmetric, and as the disease progresses, VF loss moved toward more symmetric patterns. Nevertheless, our models indicate that VF patterns of the worse eye can be used as a reference to help clinicians interpret the VF loss in the better eye. Because the ATs represent recognizable VF loss patterns and the AT decomposition protocol is publicly available,[42] our current models can be implemented in clinical practice.

Our models can accurate predict the presence of superior (AT 14, AUC: 0.89) and inferior paracentral defects (AT 16, AUC: 0.88), which may be most relevant to the quality of life of glaucoma patients given their centrality.[37,38] We have shown a clinical scenario in which paracentral defects are present, disappear, and reappear at approximate 6-month intervals (Fig. 5). If a clinician were to only have the first two tests, a third test would typically be required 6 months or so later to determine if the defect is real. Our cross-sectional model predicts that paracentral defects should be present in the better eye at each time point. The fact that the defects reappear in the third test adds validity to our model's estimation. Even with only the first two discordant tests with discordant results are available, clinicians may be reassured using our model that the defect is likely to be a true defect. Alternatively, the clinician might order 10-2 tests in the better eye to better detect paracentral loss. This is supported by previous findings that central VF loss seen on the 10-2 can often be missed on the 24-2 strategy.[25] Our models can therefore improve glaucoma monitoring. Furthermore, the clinician can better inform patients about their expected course of disease, such as if paracentral

VF loss in one eye might be followed by paracentral loss in the other eye. In terms of glaucoma treatment, there has been controversy regarding whether therapy should be started in only one eye or both eyes.[59] Given the high symmetry observed, our data support the notion that it may be reasonable to treat both eyes simultaneously even if only one eye is diagnosed with glaucoma. However, longitudinal data are needed to fully support these viewpoints.

Our findings provide valuable insight into the pathophysiology of glaucomatous optic nerve damage. The finding that VF defects present in one eye are most strongly correlated with the same type of defect pattern in the fellow eye implicates that systemic/inherited factors (e.g., gene and environment) have greater impact on glaucoma than local eye-specific factors (e.g., intereye variations of myopia severity and optic nerve head architecture), because systemic factors would likely lead to bilateral or similar VF loss patterns in fellow eyes as opposed to local eye-specific factors that would more likely produce unilateral or dissimilar VF loss patterns. Although the focus of our study is not mechanistic, our findings provide a direction for future research to find the specific determinants of this seemingly heterogeneous disease.

This study has limitations. First, this was a retrospective, cross-sectional study, so we could deduce associations at a single point in time, but not causations or longitudinal relationships. Second, our dataset only contains VF related data exported from the Humphrey Field Analyzer device. Our dataset is unlinked to any clinical data including information of glaucoma subtypes and concomitant ocular diseases that could affect intereye asymmetry. In the future, it would be interesting to further investigate how glaucoma subtypes and concomitant ocular diseases might affect the VF loss asymmetry/symmetry. Third, because VFs are subject to test-retest variability,[60,61] our models were developed based on imperfect data. However, we assume that an inherent relationship exists between fellow eyes, and, as such, our models should be able to capture the overall relationship, especially given the large dataset used in this study. Lastly, the ATs used to quantify regional VF loss include defects likely related to non-glaucomatous diseases such as age-related macular degeneration or hemianopia secondary to stroke. However, patients with glaucoma can also have comorbid eye diseases, and therefore including these VF patterns could potentially make our models more practically useful.

In conclusion, using a multicenter dataset of over 63,000 pairs of eyes, we show that strong pointwise and pattern-specific VF symmetry exists between fellow eyes. VF defects in one eye are most highly correlated with the same type of defect pattern in the other eye. We developed models to predict defects in the better eye from the VF patterns of the worse eye with higher accuracy for VF archetypes with more advanced VF loss or paracentral VF loss and lower accuracy for VF archetypes with early or mild VF loss in the peripheral region. Our findings may be used to improve disease monitoring and have implications for pathophysiology of glaucoma.

References

1. Bussel II, Wollstein G, Schuman JS. OCT for glaucoma diagnosis, screening and detection of glaucoma progression. *Br J Ophthalmol.* 2014;98(Suppl 2):ii15–ii19.

2. Garway-Heath DF, Poinoosawmy D, Fitzke FW, Hitchings RA. Mapping the visual field to the optic disc in normal tension glaucoma eyes. *Ophthalmology*. 2000;107(10):1809–1815.

3. Wang M, Jin Q, Wang H, Li D, Baniasadi N, Elze T. The interrelationship between refractive error, blood vessel anatomy, and glaucomatous visual field loss. *Transl Vis Sci Technol*. 2018;7(1):4.

4. Wang M, Elze T, Li D, et al. Age, ocular magnification, and circumpapillary retinal nerve fiber layer thickness. *J Biomed Opt*. 2017;22(12):121718.

5. Elze T, Baniasadi N, Jin Q, Wang H, Wang M. Ametropia, retinal anatomy, and OCT abnormality patterns in glaucoma. 1. Impacts of refractive error and interartery angle. *J Biomed Opt*. 2017;22(12):121713.

6. Wang M, Shen LQ, Pasquale LR, et al. An artificial intelligence approach to assess spatial patterns of retinal nerve fiber layer thickness maps in glaucoma. *Transl Vis Sci Technol*. 2020;9(9):41.

7. Baniasadi N, Wang M, Wang H, Mahd M, Elze T. Associations between optic nerve head–related anatomical parameters and refractive error over the full range of glaucoma severity. *Transl Vis Sci Technol*. 2017;6(4):9.

8. Cameron JR, Megaw RD, Tatham AJ, et al. Lateral thinking—interocular symmetry and asymmetry in neurovascular patterning, in health and disease. *Prog Retin Eye Res*. 2017;59:131–157.

9. Armaly MF. Cup/disc ratio in early open-angle glaucoma. *Doc Ophthalmol*. 1969;26(1):526–533.

10. Ong LS, Mitchell P, Healey PR, Cumming RG. Asymmetry in optic disc parameters: the Blue Mountains Eye Study. *Invest Ophthalmol Vis Sci*. 1999;40(5):849–857.

11. Qiu M, Boland M V, Ramulu PY. Cup-to-disc ratio asymmetry in US adults: prevalence and association with glaucoma in the 2005–2008 National Health and Nutrition Examination Survey. *Ophthalmology*. 2017;124(8):1229–1236.

12. Sullivan-Mee M, Ruegg CC, Pensyl D, Halverson K, Qualls C. Diagnostic precision of retinal nerve fiber layer and macular thickness asymmetry parameters for identifying early primary open-angle glaucoma. *Am J Ophthalmol*. 2013;156(3):567–577.

13. Bertuzzi F, Hoffman DC, De Fonseka AM, Souza C, Caprioli J. Concordance of retinal nerve fiber layer defects between fellow eyes of glaucoma patients measured by optical coherence tomography. *Am J Ophthalmol*. 2009;148(1):148–154.

14. Field MG, Alasil T, Baniasadi N, et al. Facilitating Glaucoma Diagnosis With Intereye Retinal Nerve Fiber Layer Asymmetry Using Spectral-Domain Optical Coherence Tomography. *J Glaucoma*. 2016;25(2):167–176.

15. Gugleta K, Orgül S, Flammer J. Asymmetry in intraocular pressure and retinal nerve fiber layer thickness in normal-tension glaucoma. *Ophthalmologica*. 1999;213(4):219–223.

16. Williams AL, Gatla S, Leiby BE, et al. The value of intraocular pressure asymmetry in diagnosing glaucoma. *J Glaucoma*. 2013;22(3):215–218.

17. Sit AJ, Liu JHK, Weinreb RN. Asymmetry of right versus left intraocular pressures over 24 hours in glaucoma patients. *Ophthalmology*. 2006;113(3):425–430.

18. Cartwright MJ, Anderson DR. Correlation of asymmetric damage with asymmetric intraocular pressure in normal-tension glaucoma (low-tension glaucoma). *Arch Ophthalmol*. 1988;106(7):898–900.

19. Greenfield DS, Liebmann JM, Ritch R, Krupin T, Group L-PGS, others. Visual field and intraocular pressure asymmetry in the low-pressure glaucoma treatment study. *Ophthalmology*. 2007;114(3):460–465.

20. Crichton A, Drance SM, Douglas GR, Schulzer M. Unequal intraocular pressure and its relation to asymmetric visual field defects in low-tension glaucoma. *Ophthalmology*. 1989;96(9):1312–1314.

21. Lee AJ, Rochtchina E, Mitchell P. Intraocular pressure asymmetry and undiagnosed open-angle glaucoma in an older population. *Am J Ophthalmol*. 2004;137(2):380–382.

22. Poinoosawmy D, Fontana L, Wu JX, Bunce C V., Hitchings RA. Frequency of asymmetric visual field defects in normal-tension and high-tension glaucoma. *Ophthalmology*. 1998;105(6):988–991.

23. Feuer WJ, Anderson DR. Static threshold asymmetry in early glaucomatous visual field loss. *Ophthalmology*. 1989;96(9):1285–1297.

24. Levine RA, Demirel S, Fan J, Keltner JL, Johnson CA, Kass MA. Asymmetries and visual field summaries as predictors of glaucoma in the ocular hypertension treatment study. *Invest Ophthalmol Vis Sci*. 2006;47(9):3896–3903.

25. De Moraes CG, Hood DC, Thenappan A, et al. 24-2 Visual fields miss central defects shown on 10-2 tests in glaucoma suspects, ocular hypertensives, and early glaucoma. *Ophthalmology*. 2017;124(10):1449–1456.

26. Fechtner RD, Weinreb RN. Mechanisms of optic nerve damage in primary open angle glaucoma. *Surv Ophthalmol*. 1994;39(1):23–42.

27. Weinreb RN, Aung T, Medeiros FA. The pathophysiology and treatment of glaucoma: a review. *JAMA*. 2014;311(18):1901–1911.

translational vision science & technology

28. Burgoyne CF, Downs JC, Bellezza AJ, Suh J-KF, Hart RT. The optic nerve head as a biomechanical structure: a new paradigm for understanding the role of IOP-related stress and strain in the pathophysiology of glaucomatous optic nerve head damage. *Prog Retin Eye Res*. 2005;24(1):39–73.

29. Quigley HA. The contribution of the sclera and lamina cribrosa to the pathogenesis of glaucoma: diagnostic and treatment implications. In: *Progress in Brain Research*, Vol. 220. Philadelphia: Elsevier; 2015:59–86.

30. Bonomi L, Marchini G, Marraffa M, Bernardi P, Morbio R, Varotto A. Vascular risk factors for primary open angle glaucoma: the Egna-Neumarkt Study. *Ophthalmology*. 2000;107(7):1287–1293.

31. Loomis SJ, Kang JH, Weinreb RN, et al. Association of CAV1/CAV2 genomic variants with primary open-angle glaucoma overall and by gender and pattern of visual field loss. *Ophthalmology*. 2014;121(2):508–516.

32. Wiggs JL, Hewitt AW, Fan BJ, et al. The p53 codon 72 PRO/PRO genotype may be associated with initial central visual field defects in Caucasians with primary open angle glaucoma. *PLoS One*. 2012;7(9):e45613.

33. Kang JH, Loomis SJ, Rosner BA, Wiggs JL, Pasquale LR. Comparison of risk factor profiles for primary open-angle glaucoma subtypes defined by pattern of visual field loss: a prospective study. *Invest Ophthalmol Vis Sci*. 2015;56(4):2439–2448.

34. Akarsu C, Yazici B, Taner P, Ergin A. Effects of moderate smoking on the central visual field. *Acta Ophthalmol Scand*. 2004;82(4):432–435.

35. Bonovas S, Filioussi K, Tsantes A, Peponis V. Epidemiological association between cigarette smoking and primary open-angle glaucoma: a meta-analysis. *Public Health*. 2004;118(4):256–261.

36. Hoffmann EM, Boden C, Zangwill LM, Bourne RR, Weinreb RN, Sample PA. Inter-eye comparison of patterns of visual field loss in patients with glaucomatous optic neuropathy. *Am J Ophthalmol*. 2006;141(4):703.

37. Abe RY, Diniz-Filho A, Costa VP, Gracitelli CPB, Baig S, Medeiros FA. The impact of location of progressive visual field loss on longitudinal changes in quality of life of patients with glaucoma. *Ophthalmology*. 2016;123(3):552–557.

38. Murata H, Hirasawa H, Aoyama Y, et al. Identifying areas of the visual field important for quality of life in patients with glaucoma. *PLoS One*. 2013;8(3):e58695.

39. Wang M, Pasquale LR, Shen LQ, et al. Reversal of glaucoma hemifield test results and visual field features in glaucoma. *Ophthalmology*. 2018;125(3):352–360.

40. Birt CM, Shin DH, Samudrala V, Hughes BA, Kim C, Lee D. Analysis of reliability indices from Humphrey visual field tests in an urban glaucoma population. *Ophthalmology*. 1997;104(7):1126–1130.

41. Newkirk MR, Gardiner SK, Demirel S, Johnson CA. Assessment of false positives with the Humphrey Field Analyzer II perimeter with the SITA Algorithm. *Invest Ophthalmol Vis Sci*. 2006;47(10):4632–4637.

42. Elze T, Pasquale LR, Shen LQ, Chen TC, Wiggs JL, Bex PJ. Patterns of functional vision loss in glaucoma determined with archetypal analysis. *J R Soc Interface*. 2015;12(103):20141118.

43. Pasquale LR, Kang JH, Manson JE, Willett WC, Rosner BA, Hankinson SE. Prospective study of type 2 diabetes mellitus and risk of primary open-angle glaucoma in women. *Ophthalmology*. 2006;113(7):1081–1086.

44. Pasquale LR, Willett WC, Rosner BA, Kang JH. Anthropometric measures and their relation to incident primary open-angle glaucoma. *Ophthalmology*. 2010;117(8):1521–1529.

45. Cai S, Elze T, Bex PJ, Wiggs JL, Pasquale LR, Shen LQ. Clinical correlates of computationally derived visual field defect archetypes in patients from a glaucoma clinic. *Curr Eye Res*. 2017;42(4):568–574.

46. Wang M, Shen LQ, Pasquale LR, et al. An artificial intelligence approach to detect visual field progression in glaucoma based on spatial pattern analysis. *Invest Ophthalmol Vis Sci*. 2019;60(1):365–375.

47. Wang M, Shen LQ, Pasquale LR, et al. Artificial intelligence classification of central visual field patterns in glaucoma. *Ophthalmology*. 2020;127(6):731–738.

48. Wang M, Tichelaar J, Pasquale LR, et al. Characterization of central visual field loss in end-stage glaucoma by unsupervised artificial intelligence. *JAMA Ophthalmol*. 2020;138(2):190–198.

49. R Core Team. *R: A Language and Environment for Statistical Computing*. 2013.

50. Benjamini Y, Hochberg Y. Controlling the false discovery rate: a practical and powerful approach to multiple testing. *J R Stat Soc Ser B*. 1995;57(1):289–300.

51. Kass RE, Raftery AE. Bayes factors. *J Am Stat Assoc*. 1995;90(430):773–795.

52. Gardiner SK, Swanson WH, Goren D, Mansberger SL, Demirel S. Assessment of the reliability of standard automated perimetry in regions

of glaucomatous damage. *Ophthalmology*. 2014;121(7):1359–1369.

53. Heijl A, Lindgren G, Olsson J. Normal Variability Of Static Perimetric Threshold Values Across The Central Visual Field. *Arch Ophthalmol*. 1987;105(11):1544–1549.

54. Blumenthal EZ, Sample PA, Berry CC, et al. Evaluating several sources of variability for standard and SWAP visual fields in glaucoma patients, suspects, and normals. *Ophthalmology*. 2003;110(10):1895–1902.

55. Gardiner SK. Differences in the relation between perimetric sensitivity and variability between locations across the visual field. *Investig Ophthalmol Vis Sci*. 2018;59(8):3667–3674.

56. Rabiolo A, Morales E, Afifi AA, Yu F, Nouri-Mahdavi K, Caprioli J. Quantification of visual field variability in glaucoma: implications for visual field prediction and modeling. *Transl Vis Sci Technol*. 2019;8(5):25.

57. Buys ES, Ko Y-C, Alt C, et al. Soluble guanylate cyclase α 1-deficient mice: a novel murine model for primary open angle glaucoma. *PLoS One*. 2013;8(3):e60156.

58. Kang JH, Willett WC, Rosner BA, Buys E, Wiggs JL, Pasquale LR. Association of dietary nitrate intake with primary open-angle glaucoma: a prospective analysis from the nurses' health study and health professionals follow-up study. *JAMA Ophthalmol*. 2016;134(3):294–303.

59. Bhorade AM. The monocular trial controversy: a critical review. *Curr Opin Ophthalmol*. 2009;20(2):104–109.

60. Heijl A, Lindgren A, Lindgren G. Test-retest variability in glaucomatous visual fields. *Am J Ophthalmol*. 1989;108(2):130–135.

61. Gillespie BW, Musch DC, Guire KE, et al. The collaborative initial glaucoma treatment study: baseline visual field and test–retest variability. *Invest Ophthalmol Vis Sci*. 2003;44(6):2613–2620.